Investigation of ultra high performance concrete piles for integral abutment bridges

By

Kam W. Ng, Ph.D.

(Corresponding Author)

Assistant Professor

University of Wyoming, Email: kng1@uwyo.edu

Jessica Garder

Assistant Structural Engineer

Burns & McDonnell; Email: jagarder@burnsmcd.com

Sri Sritharan, Ph.D.

Wilson Engineering Professor

Iowa State University, Email: sri@iastate.edu

Manuscript Published in Engineering Structures (December 2015)

1. Introduction

The depletion of natural resources, continuous deterioration of infrastructure, and increasing maintenance costs propose great challenges to the American Association of State Highway Transportation Officials (AASHTO) and many state Departments of Transportation (DOT). According to the report on grand challenges issued by the AASHTO Highway subcommittee on bridge and structures in 2005 [1], a quarter of our nation's 590,000 bridges, including their substructures and foundations, were classified as structural deficient or functionally obsolete, primarily due to material deterioration. Research areas on substructures and foundations focusing on correction protection, strengthening of piers and extending service life are encouraged. According to Lampo et al. [2] the US spent more than $1 billion annually on maintenance and replacement of conventional pile foundations that were degraded from chloride attack on concrete, steel corrosion and marine borer attack on timber.

To address these challenges the AASHTO [1], in the beginning of 2005, called for more research advancements focusing on extending service life of bridges to 75 years with minimal maintenance and optimizing structural systems using new materials. To overcome these challenges, innovative methods, such as the use of an advanced Ultra High Performance Concrete (UHPC) material that has been applied to bridge superstructures [3-7], are being investigated to extend the service life of a bridge. Since the UHPC has better durability properties than those of a conventional concrete, as measured by permeability tests, freeze-thaw tests, scaling tests, abrasion tests, resistance to alkali-silica reactivity, and carbonation, structures use UHPC are expected to have a longer service life and require less maintenance [8]. Many existing and older bridges were supported by pile foundation systems made of timber, steel and concrete. Each pile type has its advantages and limitations. Timber piles are susceptible to

damage and decay when they are installed above the water table and are subjecting to alternate wetting and drying cycle while its durability is a function of site-specific conditions. Timber pile splices are difficult to install and generally avoided. However, timber piles are recommended for the construction of bridge fender systems due to the good energy absorption properties of wood [12]. Although steel piles are commonly used in the US [9], they are vulnerable to corrosion [10], local bucking under harsh driving conditions [11], as well as the tendency to deviate from the designed location when obstructions are encountered [12]. However, steel H-piles can easily be extended or reduced in length, has strong splices to resist compression and bending, and are effective when driven into soft rock or dense materials [12]. Precast/prestressed concrete piles have relatively high breakage rate, especially when they are to be spliced [12]. Furthermore, they are susceptible to cracking as a result of large compressive and tensile stresses developed during driving [13]. However, concrete piles are usually resistant to corrosion and exhibit high load capacity [12]. When the limitations of these conventional pile foundations are facilitated by the site-specific condition and the average age of these foundations approach their service life, maintaining and replacing bridge substructures becomes a challenging task.

To minimize drivability challenges, extend a target service life, and possibly reduce maintenance costs, piles made of UHPC material can be considered as an alternative to the conventional piles. The foundation system can be optimized by utilizing the advantages of UHPC, such as 1) excellent durability characteristics as a result of small capillary porosity; and 2) very high compressive (180 MPa to 207 MPa) and tensile (12 MPa) strengths [14]. Recognizing the benefits of UHPC, the first UHPC pile research project (Phase I) was conducted in the State of Iowa, USA to understand the behavior of two 10.7 m-long UHPC piles (i.e., UHPC-1 and UHPC-2), driven in loess on top of a hard glacial till clay soil and subjected to both

vertical and lateral load tests [15]. The UHPC piles were designed with dimensions and weight similar to that of a referenced steel HP 250×85 pile (see Fig. 1). The UHPC pile section was reinforced with ten 13-mm diameter prestressing strands with no shear reinforcement. The concrete cover was reduced from 32 to 19 mm due to the high strength and durability of UHPC. The promising findings of this research summarized below provided the necessary background to advance the knowledge of UHPC piles discussed in this paper.

- The UHPC piles, with an H-shape section and the top 230-mm casted as a solid 254-mm by 254-mm block, has been successfully driven with no visible cracking using the same Delmag D19-42 hammer used to drive steel H-piles without a pile cushion.
- The average axial load capacity of the UHPC-1 was about 86% greater than that of the steel H-pile as verified using static analysis methods, dynamic analysis methods, and a static load test.
- The increase in axial pile capacity due to pile setup was observed.
- The performance of UHPC closely matched with the estimation using the LPILE software [17].

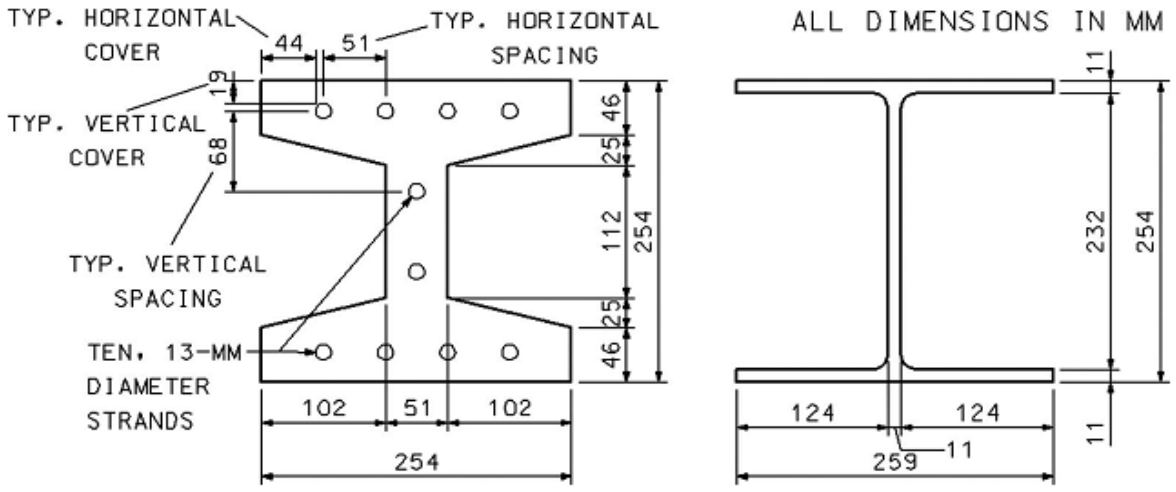

(a) H-shape UHPC pile section (b) Steel HP 250×85 pile section

Fig. 1. Cross-sectional details of a UHPC pile compared with a steel HP 250×85 pile (adopted from Suleiman et al. [15])

Recognizing the benefits of UHPC piles and the positive outcomes of Phase I research, additional research on the UHPC pile (Phase II that is discussed in this paper) was untaken to further characterize the behavior, verify the performance of UHPC piles, and facilitate the implementation of UHPC pile foundations in future bridges. Among the many objectives of the Phase II research project, this paper focuses on 1) analysis of UHPC piles in integral abutments: moment curvature and parametric analyses; 2) the production of two UHPC piles and a newly designed pile splice; 3) driveability analysis of UHPC piles with a full H-shape section; 4) the performance of the pile splice connection under a lateral load test; 5) the behavior of UHPC piles bending about both strong and weak-axes; and 6) testing the UHPC piles to failure in field.

2. Analysis of UHPC piles in integral abutments

2.1. Moment curvature analysis

The moment-curvature responses under different axial loads are required as an input in a lateral load analysis. The moment-curvature response program for UHPC piles developed by Vande Voort [14] and modified by Garder [16] is based on the following assumptions:

- Plane sections remain plane;
- Prestress losses occur due only to elastic shortening and shrinkage of UHPC;
- Strands have perfectly bonded to UHPC outside of the transfer regions;
- Effective prestressing is applied at the centroid of the section;
- Bending only occurs about the weak flexural axis;
- Initial prestressing does not induce any inelastic strains on the strands; and
- Axial loads applied through the centroidal axis of the pile.

The moment-curvature program divides the cross-section into 100 small segments and calculates the stresses and strains for each segment at a given curvature. The stress and strains are then converted into forces and moments. The prestressing, prestressing losses and axial load

contribute to the uniform strain in the concrete and are referred to as the zero curvature strains for both UHPC and prestressing steel. After the zero curvature strains are calculated, the tensile and compressive strains due to curvature are calculated. During each step, the stresses and strains are calculated for each segment of the cross-section using a stress-strain relationship of UHPC and of prestressing strands. The forces and moments are then calculated for each segment of the cross-section by manipulating the strains. The program calculates the appropriate curvature and neutral axis for each step. When the correct neutral axis is found for a curvature by satisfying the equilibrium condition, the sum of the moments in the section is equal to the total moment resistance associated with the input curvature [14]. Fig. 2 shows the moment-curvature response of the UHPC pile section in weak and strong-axes bending subjected to various axial loads. The ultimate curvature decreases with increasing axial loads. The moment in the weak-axis bending increases slightly for each load, up to 890 kN and remains the same for the axial load of 1,335 kN. The moment in the strong axis bending increases with increasing axial load. However, the amount of increase in moment decreases as the axial load increases from 890 kN to 1,335 kN. Comparing the moment-curvature responses at 890 kN, Fig. 2 shows that the flexural rigidity and the ultimate moment of a UHPC strong-axis pile are 109% greater and 56% greater than for a UHPC pile in weak-axis bending, respectively.

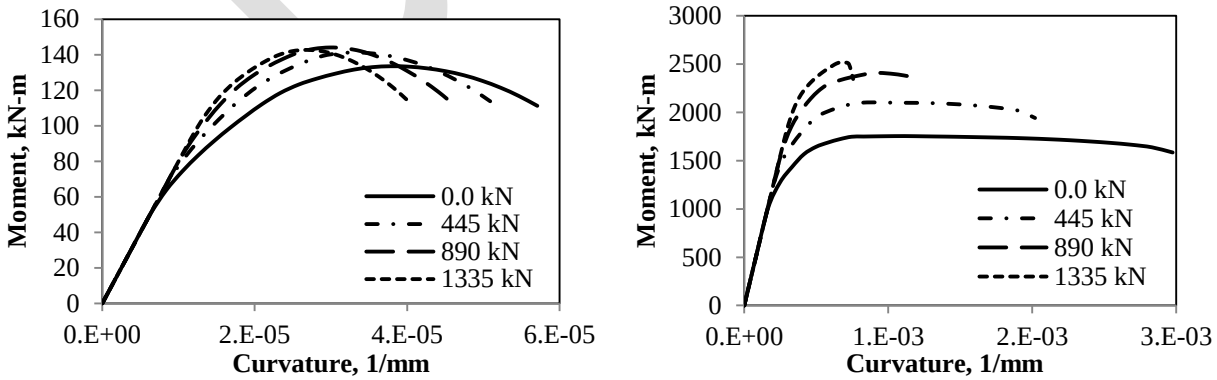

(a) Weak axis bending (b) Strong axis bending

Fig. 2. Moment-curvature of the UHPC pile section with varying axial loads

2.2. Parametric analysis

A parametric study was conducted to understand the effects of five key parameters on the lateral load performance of the UHPC piles. The estimated deflection, bending moment and shear profiles along the pile were compared for typical integral abutment pile foundation condition. These results provided the necessary technical background for selecting a test site and designing a field test for the UHPC pile as well as for future field monitoring of UHPC piles. The first parametric study was undertaken to examine the lateral load performance of a 15.24-m long UHPC pile by changing five key parameters using LPILE. Based on the variations of the five parameters listed below, a total of 128 different combinations of parameters were evaluated. Due to space limitation, selected results are presented here while completed analyses were reported by Garder [16].

- Soil Type: four soil conditions as shown in Table 1;
- Pile Head Boundary Condition: fixed and pinned;
- Axial load: 0 kN, 445 kN, 890 kN, 1,335 kN;
- Pile Orientation: weak-axis bending and strong-axis bending; and
- Lateral Displacement: 25-mm and 40-mm.

Table 1
Soil properties used for parametric analyses (adapted after Reese et al. [17])

Soil type	Density, γ (kN/m^3)	Friction angle, ϕ (degree)	Cohesion, c (kN/m^2)	Subgrade modulus, k_s (kN/m3)	Strain at 50%, $\varepsilon_{50\%}$
Loose sand	17.10	30	-	6,786	-
Dense sand	20.36	40	-	61,076	-
Soft clay	17.10	-	20.68	8,143	0.020
Very stiff clay	20.36	-	241.32	21,7158	0.004

For weak-axis bending under an axial load of 445 kN and a lateral displacement of 25-mm, Fig. 3(a) shows that the location of the second maximum moment for fixed head conditions is deeper for softer soils than stiffer soils. In very stiff clay, Fig. 3(b) shows the effect of fixed and pinned

pile head boundary conditions. The magnitude of the maximum bending moments is greater, and the location of the second peak moment and the point of fixity for the pile are deeper for the fixed pile head condition. Fig. 4(a) shows that the locations of the second maximum moment and the point of fixity remain relatively constant while the magnitude of the second maximum moment increases as the axial load increases from 0 kN to 1,335 kN. The results suggest that the effect of axial loads on the lateral performance of the pile model is negligible as the axial load will be distributed to the surrounding soil and secondary bending induced by the axial load will be very much restrained by the very stiff clay. As the orientation of the pile changes from strong-axis to weak-axis, Fig. 4(b) shows that the magnitude of the maximum and second maximum moments reduce, and the point of fixity moves closer to the pile head.

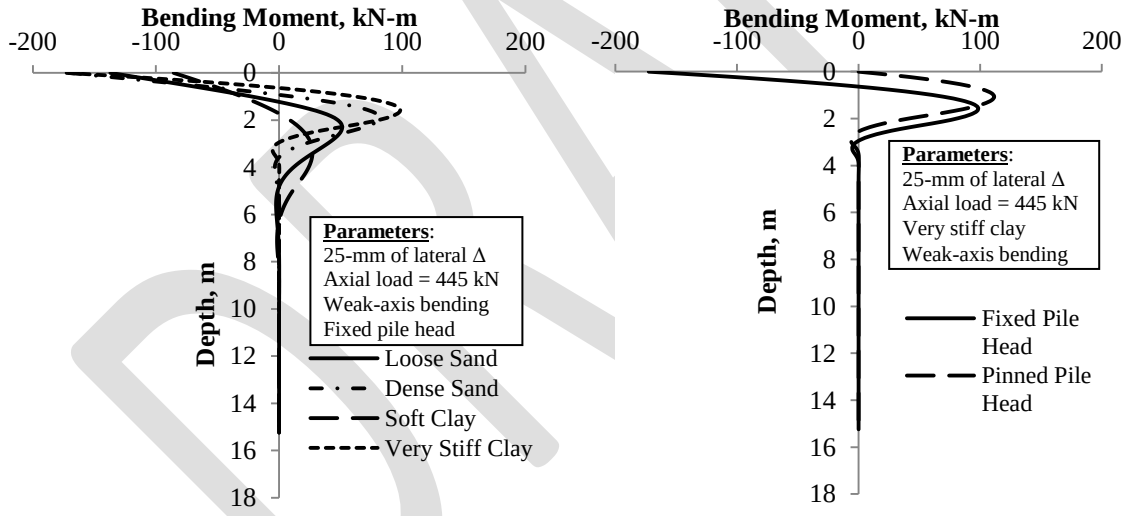

(a) Effect of soil type (b) Effect of pile head boundary condition

Fig. 3. Effects of soil type and pile head boundary condition on the moment profile of a UHPC pile

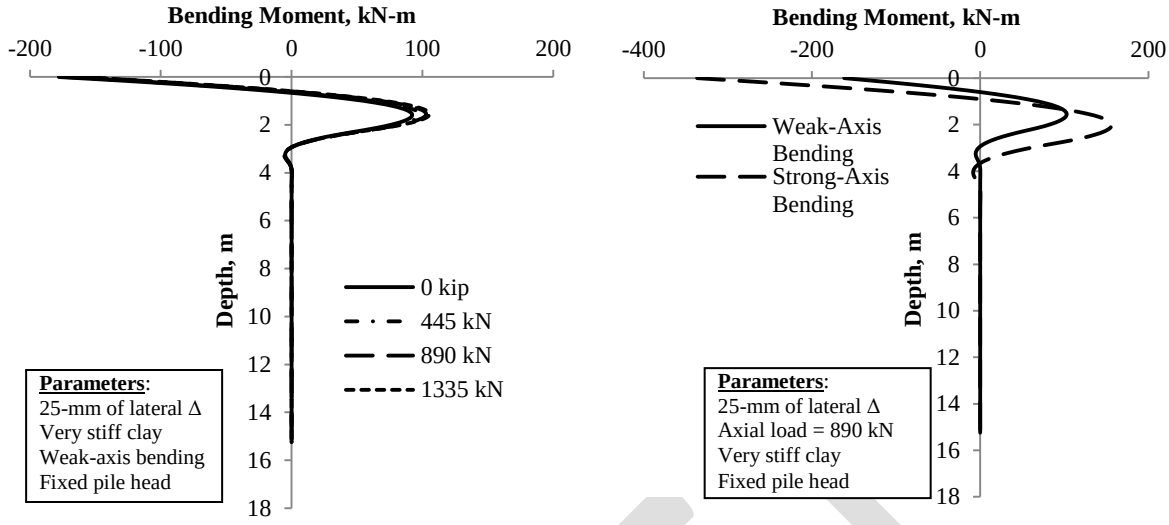

(a) Effect of axial load (b) Effect of pile orientation

Fig. 4. Effects of axial load and pile orientation on the moment profile of a UHPC pile

The second parametric study considered a 3-m deep prebore hole for piles in integral abutments as typically used in the State of Iowa when bridges exceed 40-m in length to accommodate the superstructure deformation due to temperature, creep, and shrinkage effects [18]. A total of 8 cases were evaluated for UHPC piles as given in Table 2. Weak-axis bending was selected to comply with the Iowa DOT design guidelines [18], to providing a lateral flexibility in accommodating the lateral deformation. For the specified conditions, Fig. 5 indicates that the presence of the 3-m prebore hole around the pile decreases the bending moment and increases the locations of the second maximum moment and point of fixity. This study concludes that the UHPC pile would be subjected to lateral deformations within the acceptable limits when installed in integral abutments. These parametric studies indicate the critical regions for field instrumentation and the location of potential damage along the UHPC pile. Adopting the UHPC pile section design and results obtained in Phase I as well as the results of these studies, the field testing plan described in Section 3 was developed.

Table 2

Eight cases investigated in the second parametric study considering a 3-m deep prebore hole

Conditions	Axial load (kN)	Soil type	Lateral displacement (mm)
Fixed pile head; weak-axis bending	445	Soft clay	25
			40
		Very stiff clay	25
			40
	890	Soft clay	25
			40
		Very stiff clay	25
			40

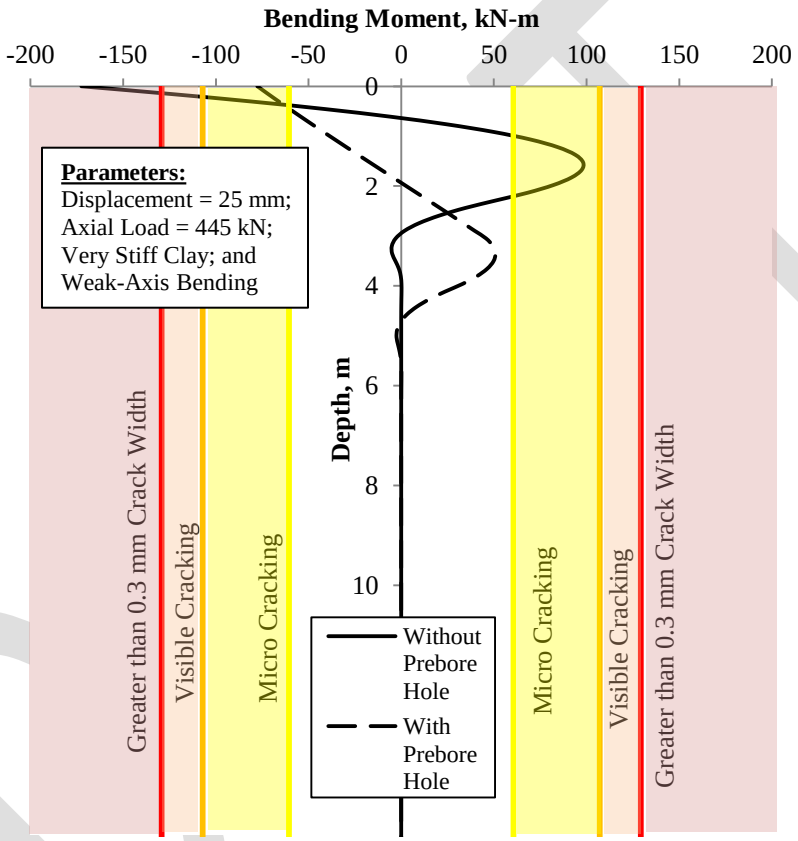

Fig. 5. Effect of a prebore hole on the imposed performance of a UHPC pile

3. Field investigation of UHPC test piles

3.1. Production, instrumentation and handling of UHPC piles

Two UHPC piles (P3 and P4), following the section design described in Phase I [14,15] and shown in Fig. 1(a), were cast at Coreslab Structures in Omaha, NE. Test pile P3 was 14-m long with a full H-shape section. Test pile P4 consists of two 4.6-m UHPC sections welded end to end

at a structural steel splice as shown in Fig. 6. The splice was made of A572 steel with a typical yield strength of 345 MPa. However, the mechanical properties of the steel used for the splice were not measured. The splice consisted of a 12.7-mm thick end plate was cut to the same dimension as the tapered H-section of the UHPC pile (see Fig. 1(a)), 10 holes were cut into the end plate to accommodate the diameter and location of the ten 13-mm diameter low relaxation prestressing strands with an ultimate strength of 1,861 MPa, and the edges of the plate were chamfered to allow for welding in the field. Additionally, 6.4-mm thick plates were bent to form the angles that were welded to each corner of the splice plate and 12.7-mm diameter shear studs were welded to the bent plates at a 127-mm spacing.

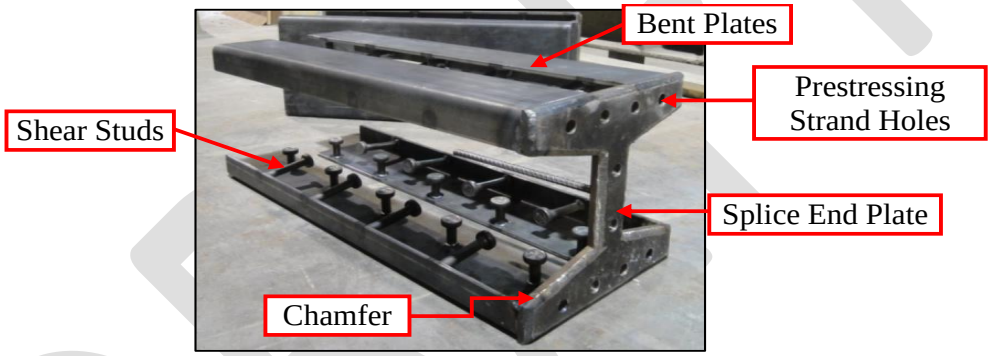

Fig. 6. UHPC steel splice

Embedded concrete strain gages were suspended between two prestressing strands that were stressed to 1,396 MPa (75% of their ultimate strength) and placed on a diagonal at each level of instrumentation, as shown in Fig. 7(a), to measure the curvature of the piles during the lateral load test. Ten pairs of gages were installed along P3 at the following depths from pile head: 1.22 m, 2.13 m, 2.74 m, 3.35 m, 3.96 m, 6.10 m, 8.53 m, 10.97 m, 13.11 m, and 13.79 m. Only three pairs of gages were installed along the second 4.6-m UHPC section (i.e., above the pile splice) of P4 at the following depths from pile head: 1.22 m, 2.74 m, and 3.91 m. Noted that most gages were installed in the top 4 m, in which the location of the second maximum moment was estimated in the parametric studies. Furthermore, 15-mm diameter steel conduits were installed

about 762-mm from each pile head to accommodate for the installation of a pair of accelerometers and strain transducers of the pile driving analyzer (PDA) during pile installation. Inclined steel brackets were used to ensure the accelerometers remained flat and tight to the pile.

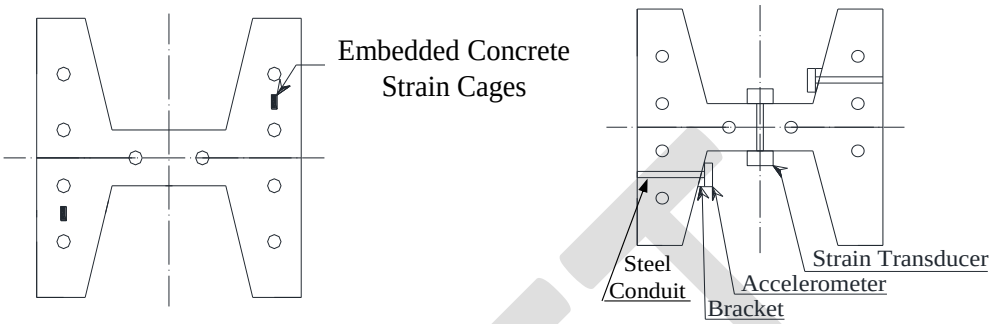

(a) Location of gages (b) Location of steel conduits

Fig. 7. Location of embedded concrete strain gages and steel conduits for PDA testing

Next, UHPC was mixed and poured into the completed forms. The top surface of the test piles were covered with plastic wraps to prevent moisture loss. Propane heaters were used for the initial curing at 30˚C. Six 76-mm diameter UHPC cylinders were cast to determine the target compressive strength of 97 MPa before the prestressing strands were cut and released. The test piles were steam cured at 90ºC for 48 hours. To help with handling the UHPC piles, lifting hooks made of #10 rebar were installed 460-mm away from both pile head and pile toe before casting. The average compressive strength of the UHPC at 28 days was 183 MPa, which satisfied a typical design compressive strength of 179 MPa. Additionally, three 1.5-m sections of the prestressing strands cut from the prestressing role used for the test piles were tested in uniaxial tension until reaching the yield stress. The average yield stress was found to be 1,727 MPa and the average modulus of elasticity was determined to be 203,044 MPa.

3.2. Location, site, and subsurface characterization

Test piles P3 and P4 were installed next to a bridge site for highway US 20 over US 71 in Sac County, IA. The bridge is a 68-m long and 12.2-m wide with a 24 degree skew. The

subsurface was characterized using a Standard Penetration Test (SPT) and a Piezocone Penetration Test (CPT_u), which was terminated at 16.75-m. The soil is primarily a Wisconsin glacial till, which consists of 1.35-m of clay overlaying a 4.15-m of clayey silty to silty clay, thin layer of silty clay to clay, and more than 12-m sandy silty to clayey silt (see Fig. 8). The ground water table was encountered at approximately 2.44-m deep. Fig. 8(a) shows the gradual increase in uncorrected SPT N-value from 8 to 15 blows per 300-mm. The average tip resistances (q_t) of the four soil layers from ground as shown in Fig. 8(b) were 1.21 MPa, 3.28 MPa, 2.99 MPa and 3.59 MPa. The average skin frictions (f_s) as shown in Fig. 8(c) are 0.05 kPa, 0.11 kPa, 0.11 kPa, and 0.07 kPa.

3.3. Installation

Two steel HP 310×79 anchor piles (RPS and RPN) were driven first on December 6 to 7, 2011 using a Delmag D16-32 diesel hammer, followed by driving P3 and then P4 on December 8, 2011 at the location indicated in Fig. 9. Although the driveability analysis described in Section 3.4 as well as positive driving responses obtained from Phase 1 [15] indicated UHPC pile stresses during driving would be well within the allowable stress values with no pile cushion at the maximum hammer stroke, the pile cushion made of 100-mm thick plywood was used for the UHPC piles as a precautionary measure. Fig. 9 indicates the total pile length and pile penetration length in ground. A shorter embedded pile length of 8.23 m for P4 was adequate to determine its lateral performance since the estimated point of fixity obtained from the parametric analysis was about 4 m. The installation process of UHPC piles was similar to that of the anchor piles. The field test was arranged to compare the UHPC piles with the steel H-piles rather than a normal strength concrete pile because steel H-pile is the most commonly used pile type in the state of Wyoming as well as in the United States [9].

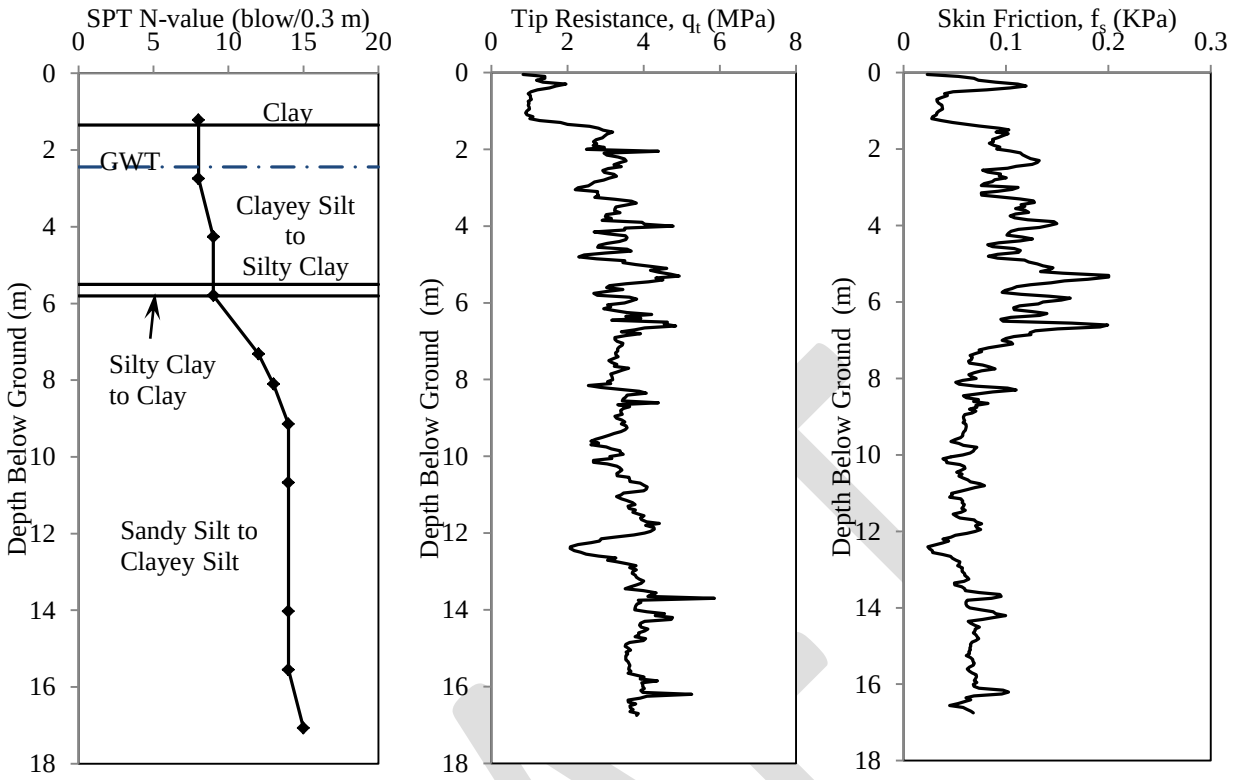

(a) SPT N-value (b) CPT-Tip Resistance (c) CPT-Skin Friction

Fig. 8. SPT and CPT data at the test pile location

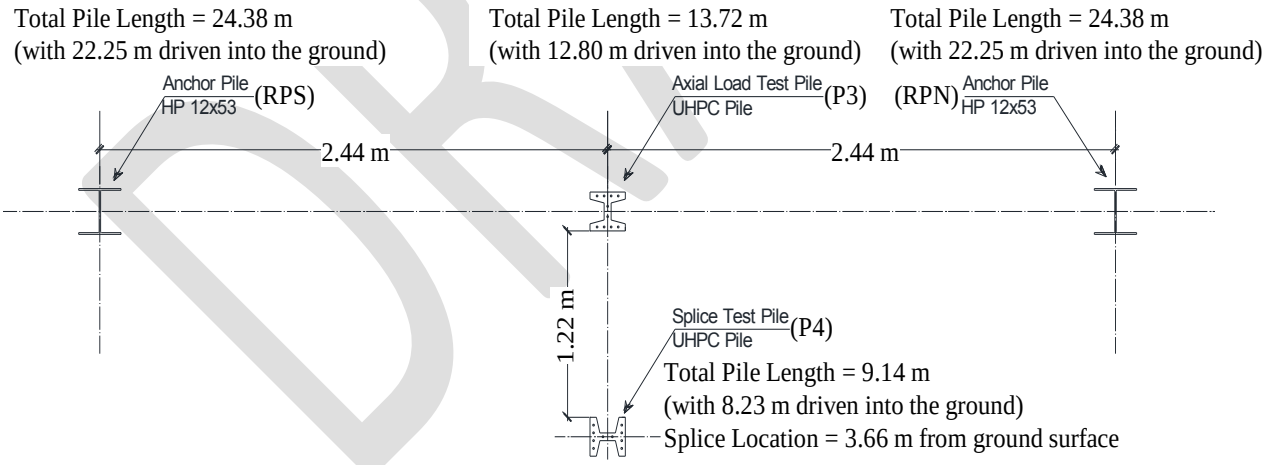

Fig. 9. Location of test piles P3 and P4 as well as steel anchor piles RPS and RPN

3.4. Driveability analysis

Prior to pile installation, a driveability analysis was conducted using GRLWEAP [19] to estimate the maximum stresses during driving for the UHPC and steel anchor piles as summarized in Table 3. PDA was used to monitor pile responses during driving, and the

measured maximum stresses were summarized. Table 3 shows that the predicted and the measured maximum stresses of all piles are well below the allowable driving limits calculated in accordance with the AASHTO Specifications [20]. No visible structural damage to all piles was observed after driving. Notably, the driveability analysis concludes that the UHPC test piles performed extremely well during driving.

Table 3
Maximum stresses during driving of the UHPC and steel anchor piles

Pile	Stress	Predicted stresses using GRLWEAP (MPa)	Measured stresses using PDA (MPa)	Allowable driving limits (MPa)
RPS	Compressive	203	197	310[a]
	Tensile	12	8	310[a]
RPN	Compressive	203	212	310[a]
	Tensile	12	12	310[a]
P3	Compressive	50	37	122[b]
	Tensile	0.7	1.4	37[c]
P4	Compressive	41	39	122[b]
	Tensile	0.0	0.7	37[c]

[a] = $0.9f_y$; [b] = $0.85f'_c - f_{pe}$; [c] = 6.9 MPa + f_{pe}; where f_y = yield strength of steel (345 MPa), f'_c = compressive strength of UHPC; and f_{pe} = effective prestressing after losses.

3.5. Dynamic restrike test

Five restrikes were performed on P3 and P4 at approximately 8 minutes, 20 minutes, 1 hour, 4 days and 6 days after the EOD. Six restrikes were performed on the anchor piles at approximately 8 minutes, 20 minutes, 1 hour, 1 day, 5 days, and 7 days after the EOD. The objective of performing a series of dynamic restrike tests is to evaluate the effect of pile setup on the increase in axial pile capacity. The results of the dynamic restrike tests both UHPC piles and anchor piles are presented as a percent increase in the pile resistance with respect to the resistance estimated by CAPWAP at the EOD in Fig. 10. All four piles experienced pile setup with pile resistances increased logarithmically as a function of time immediately after the EOD. The slope of the best fit line describes the rate of pile setup, and P3 experienced the highest rate of pile setup. Also, P3 experienced the highest pile setup with 98% increase in the pile resistance estimated by CAPWAP and 110% measured by the static load test described in Section 3.6.

Although the embedded lengths of P3 (12.8 m) and P4 (8.2 m) were shorter than the anchor piles (22.3 m), the pile setup rate of the UHPC piles were higher. Also, the percent increase in pile resistance of P3 was higher than both anchor piles. This observation was attributed to a larger cross-sectional area of 364.5 cm^2 of the UHPC pile as compared with 100 cm^2 of the anchor pile (see Fig. 1). A larger cross-sectional area exerted a greater disturbance to the surrounding soil during the pile installation and eventually caused a larger pile setup.

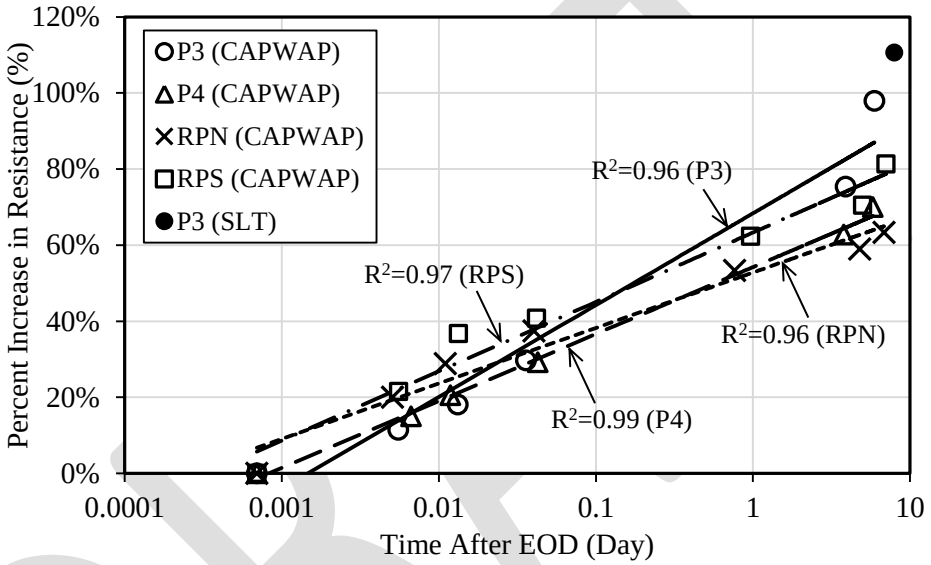

Fig. 10. Percent increase in pile resistance as a function of time after the EOD

3.6. Vertical load test

Immediately after all restrikes, vertical load test was performed on P3 using the test setup shown in Fig. 11. A load was applied on P3 by applying an equal and opposite load on the main reaction beam, from which the load was transferred to the two anchor piles and then the surrounding soil via skin friction. Four 250-mm stroke displacement transducers mounted on independent, wooden reference beams were used to measure the vertical displacement at the top of P3. The vertical load test was completed following "Procedure A: Quick Test" outlined in ASTM D1143 [21], in which P3 was loaded in 5% increments up to the anticipated failure load of 890 kN estimated using the Iowa DOT Blue Book method [23]. Fig. 12 shows that the soil-

pile system remained in the linear-elastic range although the applied load reached 890 kN. The pile was continuously loaded until experiencing excessive vertical displacement. After the maximum load was reached P3 was unloaded in 10% decrements. The pile capacity was determined to be 1,321 kN based on the Davisson failure criterion [22] given by

$$\Delta_{\text{Davisson}}(\text{mm}) = \frac{\text{PL}}{\text{AE}} + 3.81 + \frac{\text{D}}{3048} \quad (1)$$

where P is the axial load (kN), L is the pile length (mm), A is the cross-sectional area (mm^2), and E is the modulus of elasticity (kN/mm^2). The Davisson criterion was selected because it is the major pile capacity determination method used in the Load and Resistance Factor Design (LRFD) of deep foundations and has been adopted in the AASHTO Specifications [20]. The measured strains from the embedded strain gauges were used to calculate the load transfer along P3. Based on the load transfer at the ultimate pile capacity of 1,321 kN, the total side resistance and end bearing were determined to be 1,234 kN and 87 kN, respectively. Compared with the 1,321 kN obtained from the static load test, Table 4 shows that the total pile capacity estimated using the Iowa Blue Book was underestimated by 33%, while PDA and the signal matching analysis using the CAse Pile Wave Analysis Program (CAPWAP) [24], based on the last dynamic restrike test, provide a relatively good pile capacity estimation. Similar pile capacity estimations were performed on the steel anchor pile RPS as summarized in Table 4. Although higher total capacities were anticipated for RPS, which has a longer embedded pile length of 22.25 m, UHPC test pile P3 has higher total pile capacity per unit length, ranging by 31% to 38%. This comparison further suggests that the application of UHPC piles will reduce the total pile length in a foundation system. The results suggest the feasibility of using the UHPC pile when the pile performance in terms of its capacity will be verified in the field using the

PDA/CAPWAP. This promising agreement also provides the basis for future research that would consider different aspect ratios and soil profiles.

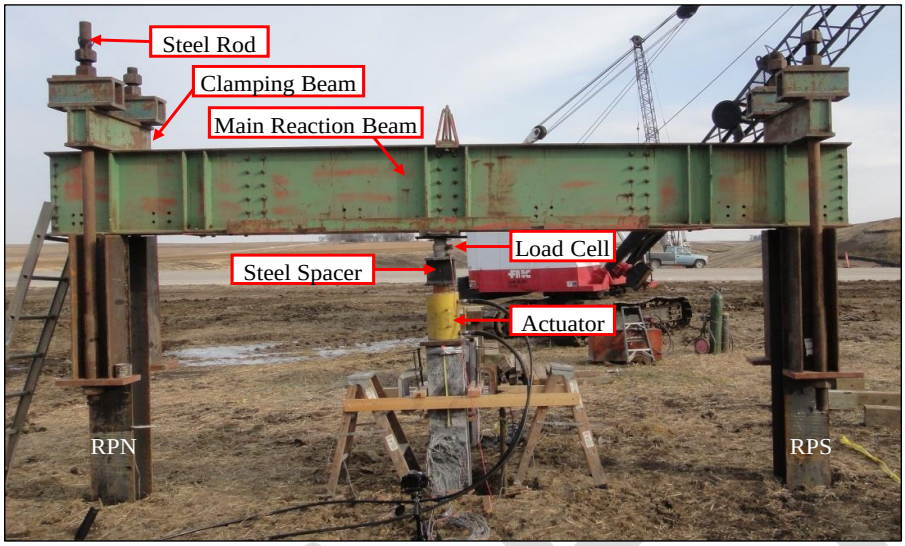

Fig. 11. Completed vertical load test setup

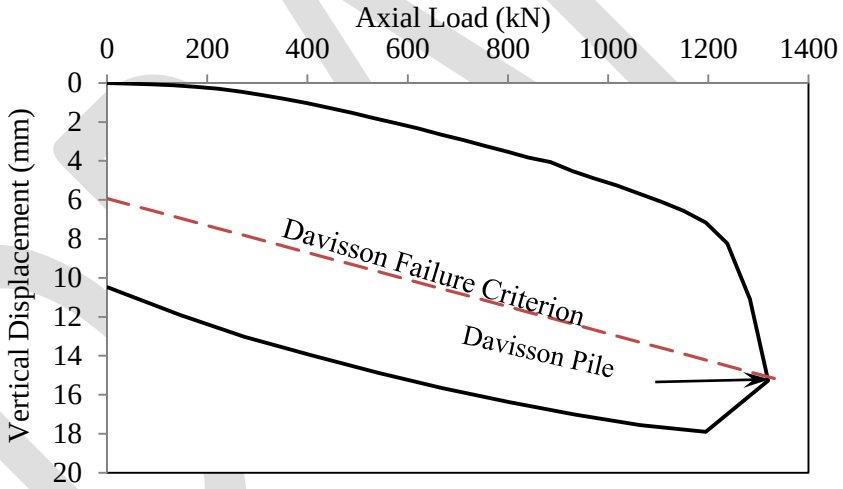

Fig. 12. Vertical load-displacement curve and Davisson failure criteria

Table 4
Comparison of pile capacities of UHPC pile P3 and steel anchor pile RPS

Method	UHPC P3 (12.8 m into ground)				RPS (22.3 m into ground)			
	Side resistance (kN)	End bearing (kN)	Total capacity (kN)	Total capacity per meter (kN/m)	Side resistance (kN)	End bearing (kN)	Total capacity (kN)	Total capacity per meter (kN/m)
Iowa Blue Book	704	186	890	70	997	167	1164	52
PDA (LS)	1361	0	1361	106	1032	672	1704	77
CAPWAP (LS)	1111	128	1239	97	1411	232	1643	74
Static load test	1234	87	1321	103	-	-	-	-

LS = last restrike.

3.7. Lateral load test

Three days after completing the vertical load test, a lateral load test was performed on P3 with a strong-axis bending as well as on P4 with a weak-axis bending and a splice at 4.57 m from pile head. The lateral load test was performed after the vertical load test to minimize the effect of test sequence on the lateral performance of the UHPC piles. The completed lateral load test setup is shown in Fig. 13. The lateral load was applied using a 445 kN actuator placed approximately 800-mm above ground. Along the line of the lateral load, two 254-mm stroke displacement gages, mounted to independent, wooden reference beams behind each test pile, were used to measure the lateral displacement of each pile. The lateral load test was performed following "Procedure A: Standard Loading" of ASTM 3966-07 [25]. For the first load cycle, both piles were loaded up to 200% of the proposed lateral design load of 45 kN unless failure occurs first. For the remaining three cycles, the piles were displacement controlled based off the measurements taken from P4 at 100-mm, 178-mm, and 254-mm. Between each cycle the UHPC test piles were unloaded to 0 kN of lateral load. Fig. 14 shows that P4 with a greatly reduced lateral stiffness as shown in Fig. 2 displaced about five times (211-mm) more than that of P3 (43-mm) at the maximum lateral force of 92 kN during the 1st cycle. The lateral force-displacement curves for the remaining cycles of P3 shown in Fig. 14(a) are within the force-displacement loop of the 1st cycle, and the final residual displacement was significantly small. In contrast, P4 had a maximum displacement of 254-mm and exhibited a relatively large final residual displacement of 60 mm, which was confirmed by a noticeable heaving of the soil on one side of P4 during the test. The increase in stiffness at about 200 mm, especially observed in P4 shown in Fig. 14(b), was attributed to the continuous densification of the surrounding top soil layer during the three cycles of lateral loading and the contribution of soil stiffness to the pile system when P4 was

pushed through the void distance of about 200 mm created from previous load tests before exerting against the soil as illustrated in Fig. 13.

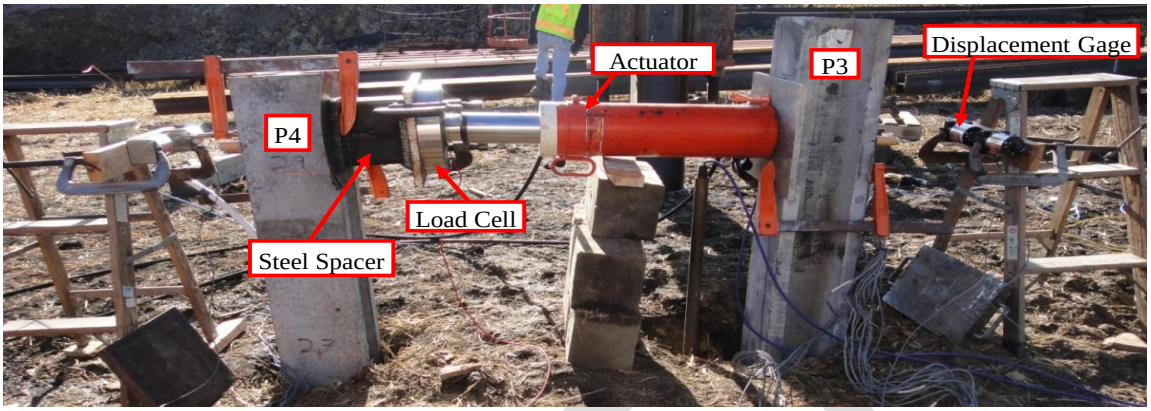

Fig. 13. Completed lateral load test setup

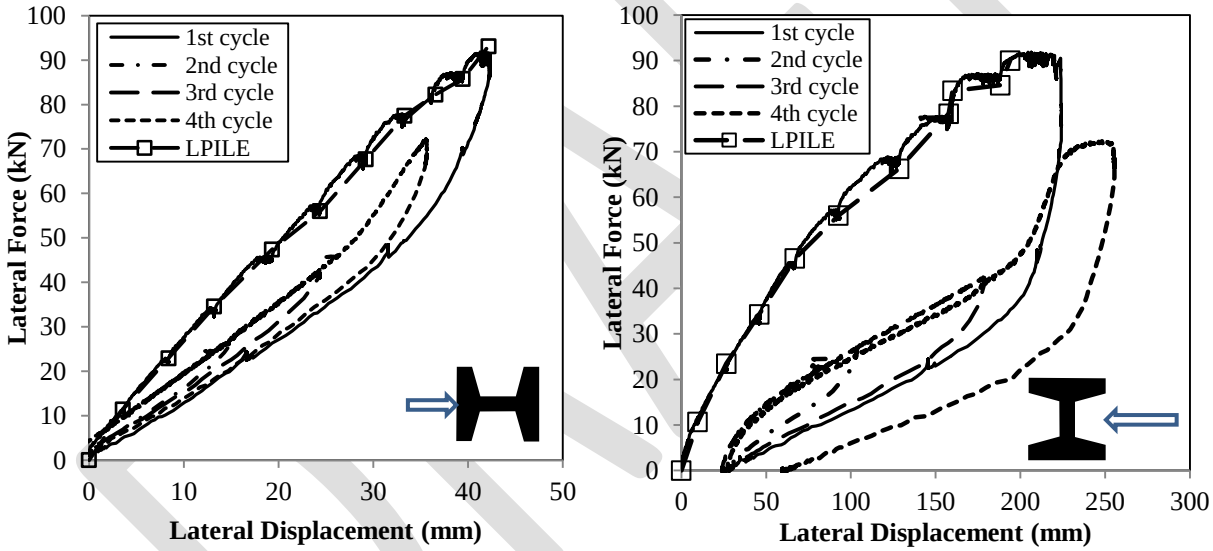

(a) P3: strong-axis bending (b) P4: weak-axis bending

Fig. 14. Lateral force-displacement responses measured during lateral load test and estimated using LPILE

LPILE was used to simulate the lateral force-displacement behavior of P3 and P4 during the lateral load test. The average undrained shear strengths (S_u) calculated from the CPT data and the moment-curvature response calculated for strong-axis and weak-axis bending at 0 kN axial load were used as input values into LPILE. Fig. 14 shows good match between the LPILE estimated and field measured lateral load-displacement responses for both P3 and P4.

Additionally, pile response in terms of moment estimated using the LPILE was compared with the average measured values of P3 and P4 at the 55.6 kN load step as shown in Fig. 15 and Fig. 16, respectively. The average moments were calculated from the tension and compression strains which were then averaged. Both figures show a good match of LPILE estimated and field measured moments. At the 55.6 kN lateral load, P3 was predicted to perform well below the threshold of having micro-cracking as illustrated in Fig. 15, while P4 was predicted to have crack widths greater than 0.3 mm as illustrated in Fig. 16. After completing the lateral load test, soil surrounding P4 was excavated 4 m below the ground level to expose the splice as shown in Fig. 17. The soil remained on the pile surface, especially in the void spaces along the web, was removed. The pile surface was clean with wet towels from covering with soil to allow a good visual inspection. A flexural crack was observed 2.74 m from the pile head on the tension side of P4 as shown in Fig. 18. The crack location agreed with the maximum moment location predicted in LPILE as presented in Fig. 16.

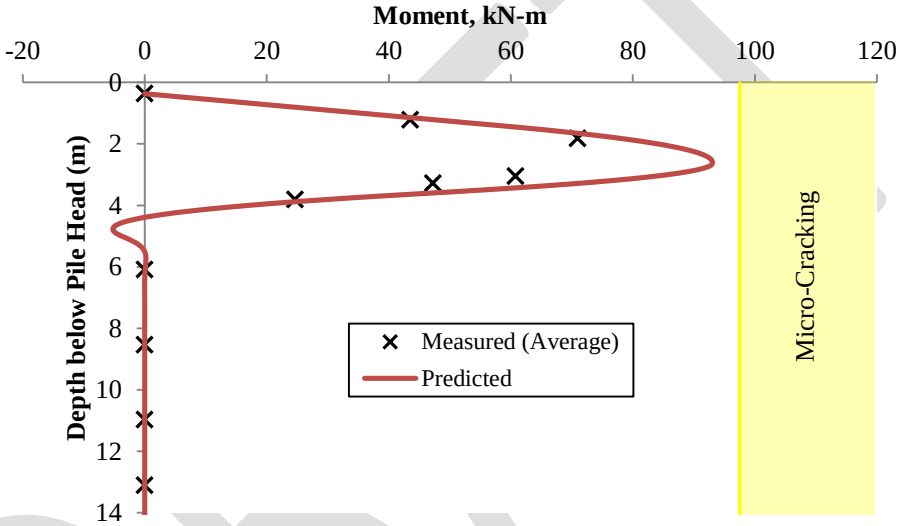

Fig. 15. Estimated and measured moments along the length of P3 at the 55.6 kN load step during the lateral load test

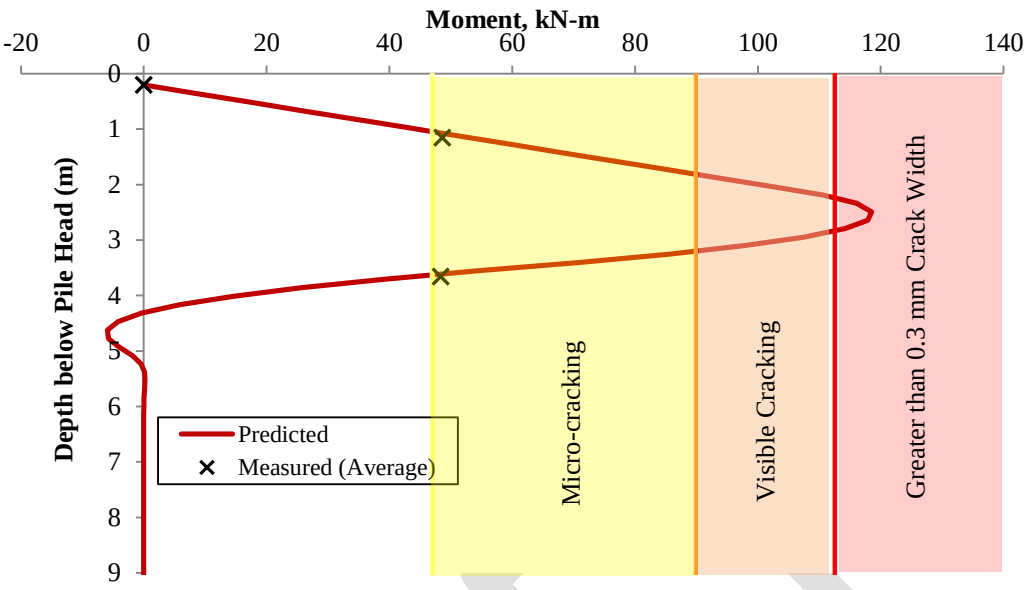

Fig. 16. Estimated and measured moments along the length of P4 at the 55.6 kN load step during the lateral load test

Fig. 17. Excavation of soil surrounding P4

Fig. 18. A flexural crack found at a depth of 2.74 m below the top of P4

3.8. Splice Performance

The structural splice on P4, which was located 4.57 m from the pile head and driven to 3.66 m below the ground surface, performed well during installation. The maximum compressive stress of 39 MPa and the maximum tensile stress of 0.7 MPa are significantly smaller than the allowable driving limits of 122 MPa and 37 MPa, respectively, as indicated in Table 3. Also, no damage was detected by the PDA during driving and restrike tests as the integrity factors (BTA) that describe the degree of convergence of measured pile force and velocity records were 100%. During the lateral load test, the splice was subjected to 5.92 kN-m bending moment as shown in Fig. 16 and a shear force of 11.6 kN as shown in Fig. 19. The splice proved to be very robust with a reserve shear capacity of 200 kN, which exceeds the maximum shear demand from the lateral load field test of 91.6 kN by 218 percent [26]. Thus, the performance of the splice in the field can be expected to meet the required shear and moment demands. Careful visual inspection was conducted by all authors on site to identify cracks and fractures on both the splice and UHPC in the vicinity of the splice. No damage was observed on or near the splice. Unfortunately, non-destructive methods were not available to detect any micro-scale crack on and near the splice.

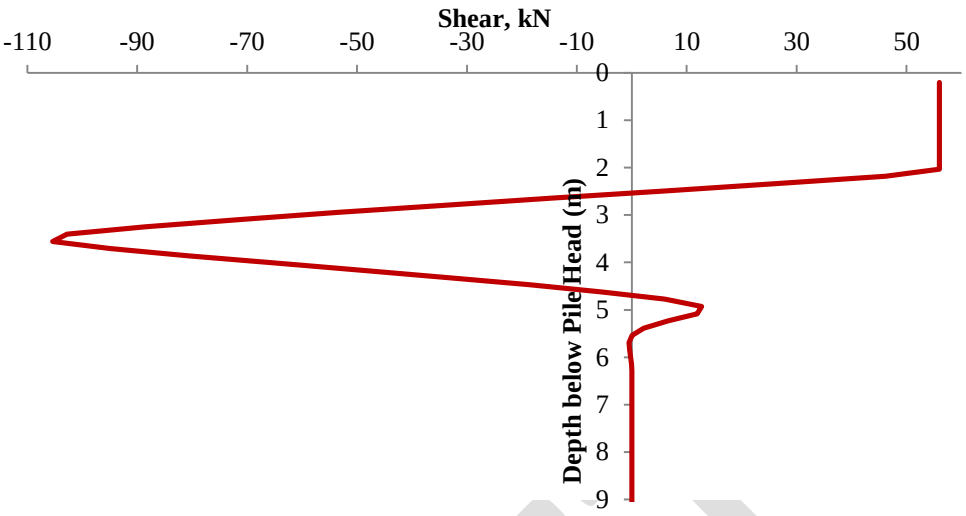

Fig. 19. Estimated shear along P4 during 55.6 kN load step of lateral load test

4. Conclusions

The paper further verifies the design analysis, fabrication and installation of UHPC piles in comparison to the typically used steel H-piles for integral abutment bridges. The major outcomes of this research are summarized as follows:

1) The parametric study of the UHPC pile suggested that the UHPC pile could be considered as an alternative foundation option for integral abutment bridges. The adequate vertical and lateral performances of the UHPC piles and its resistance to driving during pile installation further facilitate the application of UHPC as an alternative to the conventional pile systems.
2) The parametric study revealed that the 3-m prebore hole, required by Iowa DOT at the integral bridge abutment to eliminate any downdrag forces around the pile, decreased the bending moment and minimized cracking to an acceptable level during the cyclic expansion and contraction of the bridge due to thermal movements.

3) Driveability analysis performed using WEAP concluded that the measured maximum stresses of UHPC piles were well below the allowable driving limits. The UHPC test piles performed extremely well during driving.
4) The static load test results concluded that the UHPC test pile has higher total pile capacity per unit length than that of a steel H-pile. This conclusion suggests that the application of UHPC piles could enhance the efficiency of the foundation construction by reducing the total pile length of the foundation system or reducing the number of piles needed in a pile group.
5) The lateral load test results confirmed that P4 with a greatly reduced lateral stiffness displaced about five times more than that of P3. The lateral force-displacement curves for the remaining cycles of P3 shown in Fig. 14(a) are within the force-displacement loop of the 1st cycle, and the final residual displacement was significantly small. Additionally, P4 exhibited a relatively large final residual displacement than P3.
6) The numerical analysis using LPILE provided a good match of the measured lateral load test results.
7) The pile splice performed well during installation and no visible damage was found after driving. The structural performance of the splice exceeded the required shear, moment, and tensile demands.
8) The experiment results presented in this paper provide the technical background knowledge of using UHPC piles. Although limited UHPC piles were tested, the promising results provide the basis for future research that would consider different pile aspect ratios and soil profiles. Also, other factors, such as material supplies and costs, manufacturing procedures and costs, local design and construction practices and

specifications development, should be investigated in the future by different agencies from different geological regions before the UHPC piles can be widely implemented and be recognized as a viable foundation system despite its relatively durable characteristics.

Acknowledgments

This research project was sponsored by the Iowa Highway Research Board through seed funding for high-risk research ideas. The authors would like to thank the technical advisory committee of the research project. Special thanks are due to Lafarge North America, Coreslab Structures, Inc. of Omaha, Howe's Welding of Ames, Iowa State Ready Mix Concrete, and Graves Construction Co, Inc. of Spencer, IA.

References

[1] AASHTO Highway Subcommittee on Bridges and Structures. Grand Challenges: A Strategic Plan for Bridge Engineering. Washington DC; 2005.

[2] Lampo R, Maher A, Busel JP, Odello R. Design and Development of FRP Composite Piling Systems. Proceedings of the International Composites Expo, Nashville, TN; 1997.

[3] Behloul MR. Ductal® Prestressed Girders for a Traffic Bridge in Mayenne, France. 7th International Conference on Short & Medium Span Bridges, Quebac, Canada; 2006.

[4] Wipf TJ, Phares BM, Sritharan S, Degen BE, Giesmann MT. Design and Evaluation of Single-Span Bridge Using Ultra High Performance Concrete. Final Report. Center for Transportation Research and Education, Iowa State University; 2009.

[5] Perry VH, Seibert PJ. Working with Ductal Ultra-High Performance Concrete. Concrete Plant International, North American Edition; February 2011.

[6] Ozyildirim C. Evaluation of Ultra High Performance Fiber Reinforced Concrete. Final Report. Virginia Center for Transportation Innovation & Research. Charlottesville, VA; 2011.

[7] Federal Highway Administration (FHWA). Focus–Ultra High Performance Concrete: Taking Concrete to New Levels; March 2011.

[8] Russell HG, Graybeal BA. Ultra-High Performance Concrete: A State-of-the-Art Report for the Bridge Community. Report No. FHWA-HRT-13-060, Federal Highway Administration, Washington, DC; 2013.

[9] AbdelSalam SS, Sritharan S, Suleiman MT. Current Design and Construction Practices of Bridge Pile Foundations with Emphasis on Implementation of LRFD. Journal of Bridge Engineering 2010; 15(6): 749-758.

[10] White DJ, Mekkawy MM, Sritharan S, Suleiman M. Underlying Causes for Settlement of Bridge Approach Pavement Systems. Journal of Performance of Constructed Facilities, ASCE 2007; 21(4): 273-282.

[11] Huck RW, Hull JR. Resonant Driving in Permafrost. Foundation Facts, 1971; 7(1): 11-15.

[12] Hannigan PJ, Goble GG, Thendean G, Likins GE, Rausche F. Design and Construction of Driven Pile Foundations – Volumn I, FHWA-NHI-05-042. National Highway Institute, Federal Highway Administration, U.S. Department of Transportation, Washington, D.C; 2006.

[13] Salgado R. The Engineering of Foundations. McGraw-Hill, 2006.

[14] Vande Voort TL, Suleiman MT, Sritharan S. Design and Performance Verification of UHPC Piles for Deep Foundations. Final Report. Center for Transportation Research and Education, Iowa State University, Ames, IA; 2008.

[15] Suleiman MT, Vande Voort T, Sritharan S. Behavior of Driven Ultrahigh-Performance Concrete H-Piles Subjected to Vertical and Lateral Loadings. Journal of Geotechnical and Geoenvironmental Engineering 2010; 136(10): 1403-1413.

[16] Garder J. Use of UHPC Piles in Integral Abutment Bridges. MS Thesis. Department of Civil, Construction and Environmental Engineering, Iowa State University, Ames, IA; 2012.

[17] Reese LC, Wang ST, Isenhower WM, Arrellaga JA. Computer Program: LPILE Version 4 Technical Manual, Ensoft, Austin, TX; 2000.

[18] Iowa Department of Transportation. Iowa LRFD Bridge Design Manual. Retrieved February 2012, from Iowa DOT Design Policies; 2011.

[19] Pile Dynamics, Inc (PDI). GRLWEAP – Wave Equation Analysis of Pile Driving, Procedures and Models. Cleveland, OH; 2005.

[20] American Association of State Highway and Transportation Officials (AASHTO). AASHTO LRFD Bridge Design Specifications. Fifth Edition, Washington, DC; 2010.

[21] American Society for Testing and Materials (ASTM) D1143-07. Standard test methods for deep foundations under static axial compressive load. West Conshohocken, PA; 2007.

[22] Davisson MT. High Capacity Piles. Proceedings, Soil Mechanics Lecture Series on Innovations in Foundation Construction, ASCE, New York 1972: 81-112.

[23] Dirks KL, Kam P. Foundation Soils Information Chart: Pile Foundation. Iowa Department of Transportation: Highway Division-Soils Survey Section, Ames; 1994.

[24] Pile Dynamics, Inc. (PDI). CAPWAP for Windows Manual. Cleveland, Ohio; 2000.

[25] American Society for Testing and Materials (ASTM) D3966-07. Standard Test Methods for Deep Foundations under Lateral Load. West Conshohocken, PA; 2007.

[26] Sritharan S, Aaleti S, Bierwagen D, Garder J, Abu-Hawash A. Current Research on Ultra High Performance Concrete (UHPC) for Bridge Applications in Iowa. Proceedings of the 3rd International Symposium on UHPC and Nanotechnology for High Performance Construction Materials, Kassel, Germany, 2012: 857-864.